A feasibility investigation of a small scale magnetically assisted torsion pendulum gravitational wave detector

Will the MAGPI fly?

Tyson Jones

Semester 2, 2015

Abstract

Current linear pendulum gravitational wave detectors have undesirably large resonant frequencies and observe at $\geq 10\,\text{Hz}$, below which their reception of g-waves is obfuscated by a strong response to seismic noise. These detectors thus fail to detect a bandwidth of smaller frequencies associated with many interesting astrophysical phenomenon. A linear pendulum's resonant frequency is insensitive to changes in pendulum length, but a torsion pendulum's resonant frequency is much more easily modulated. The proposed magnetically assisted gravitational-wave pendulum intorsion (MAGPI) uses magnetic assistance to sustain an asymmetric torsion pendulum which can couple to gravitational waves in the millihertz band. The feasibility of a small-scale MAGPI implementation was here investigated across several design iterations, and a physical configuration is proposed.

1 Acknowledgements

I express immense gratitude toward Eric Thrane, Lincoln Turner and Russell Anderson for their endless patience, insight and guidance. Thanks also to Csaba Balaz for clarification of non-cartesian generalised forces.

Contents

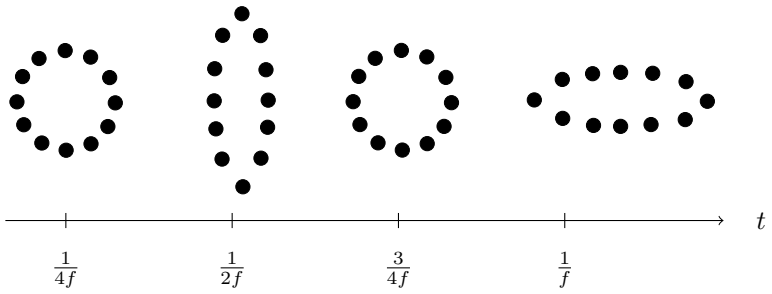

Figure 1: Visualisation of exaggerated orthogonal, oscillating space strains from a passing gravitational wave through the page, of frequency f. Four instances in time are displayed across the period of the wave (alignment with the time axis is arbitrary), and show alternating horizontal and vertical contraction and elongation.

2 Introduction

2.1 Gravitational Waves

For almost a century, Einstein's field equations have provided a theoretical basis for the existence of gravitational waves; propagating, quadrupolar deformations of space. Gravitational waves incur a compression of space in a direction orthogonal to the wave's propagation, and elongation in the direction orthogonal to both, alternating at the frequency of the wave [1].

A gravitational wave incident on a system of free particles causes apparent oscillatory motion in the orthogonal plane, as visualised in Figure 1. At a particular region in space, we model the space-strain due to a passing wave as sinusoidal in each of the propagation-orthogonal directions.

2.2 Astrophyiscal Motivation

The union of General Relativity and Astrophysics has presented a variety of potential sources of gravitational waves.

With current detector technologies, black holes, low-mass X-ray binaries (two star systems luminous in X-rays), fast pulsars (rapidly rotating, magnetised neutron stars) and many more astrophysical phenomenon can be studied by detection of their emitted *high-frequency* gravitational waves [2]; waves with frequencies within 1–10^3 Hz.

However, many interesting astrophysical events produce gravitational waves in the *low frequency band* 10^{-4}–1 Hz, below the audible band of these detectors. These include massive black hole mergers (merging black holes of mass 10^4–10^7 solar masses), extreme-mass-ratio inspirals (the inspiral of massive, compact objects like white dwarfs, neutron stars and stellar mass black holes into massive black holes) and even early cosmological processes [3, p. 228].

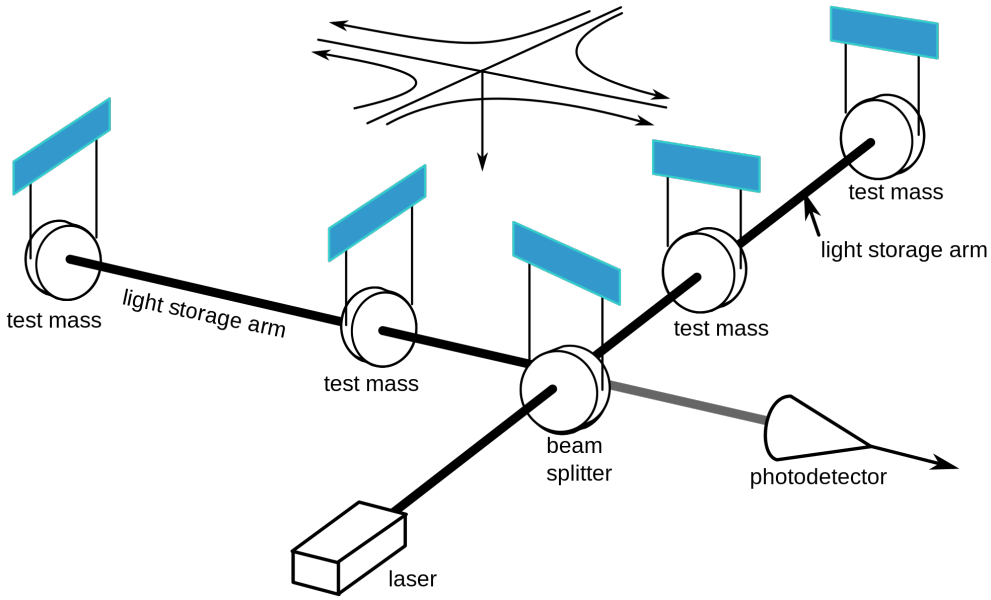

Figure 2: A laser Michelson interferometer between linear pendulums, as employed in LIGO for gravitational wave detection [4]. The quadrupolar nature of an incident gravitational wave (visualised above the detectors) sees an anticorrelated strain in the orthogonal light storage arms to which the Michelson interferometer is most sensitive, leading to detectable interference at the photodetector [1].

2.3 Current Detectors

Current gravitational wave observatories, such as the LIGO facilities, feature a laser Michelson interferometer between pairs of linear pendulums (see Figure 2), the bobs of which act as free-masses (referred to as the *test masses*) upon which mirrors are fixed.

A gravitational wave passing through the interferometer, at a particular instance in time, elongates the space between the pair of test masses in one arm and compresses the space between the other. This leads to detectable interference of the laser light at the photodetector. Over time, the alternating nature of the gravitational wave strain produces oscillatory interference from which the gravitational wave is analysed [4].

Even the Advanced LIGO detectors however observe only in the 10–100 Hz band [5] due to an attenuated gravitational-wave response and strong mechanical response of the pendulums to obfuscating, extraneous noise forces at lower frequencies. This is an artefact of the mechanics of linear pendulums which see little response to below-resonant frequency driving forces at their masses but strong response to those at their suspension point, where gravitational strains and mechanical noises (such as seismic) 'act' respectively.

Since the resonant frequency of a linear pendulum varies inversely with the root of its arm length, a reduction in resonant frequency from 1 Hz to 1 mHz would require a physically infeasible factor

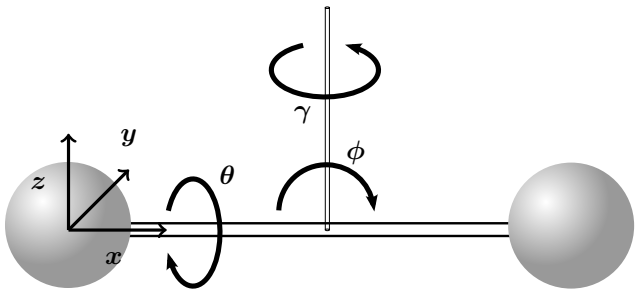

Figure 3: Visualisation of the adopted cartesian axis and yaw (γ), roll (ϕ) and pitch (θ) rotational axes about the torsion pendulum. The origin lies at the left end of the pendulum arm, when suspended parallel to the ground (the center of any attached mass or magnet at that point). The z axis is vertical and the y axis extends into the image.

10^6 expansion in vertical arm length. This insensitivity places a strict lower limit on the resonant frequency of terrestrial linear pendulum detectors and their resulting gravitational-wave detection band.

2.4 The MAGPI

Torsion pendulums may swing like linear pendulums, but offer additional axes of rotation as illustrated in Figure 3, to which gravitational-waves may couple. Of particular usefulness, torsion pendulums offer resonant yaw frequencies inversely proportional to the root of their moment of inertia about the yaw axis (their lower suspension point). Since the pendulum arm is lateral, this moment of inertia can be increased (and the resonant yaw frequency decreased) by a relatively easy increase in arm length or changes in mass distribution along the arm.

However, static suspension of an otherwise unassisted torsion pendulum requires its center of mass be at its lower suspension point, otherwise Earth's gravitational field exerts a net rolling torque. In this static setup, an incident gravitational wave, acting at the center of mass, would incur a zero yaw torque on the pendulum, causing it so swing as if it were linear.

The magnetically assisted gravitational-wave pendulum intorsion (MAGPI) design features an asymmetric torsion pendulum with an attached permanent magnet and a center of mass apart from the suspension point, allowing gravitational wave coupling. This is illustrated in Figure 4. The gravitational roll torque is countered by a magnetic torque, produced by the fixed magnet's interaction with an external magnetic field. The MAGPI constitutes a stable, gravitational-wave coupling, low resonant frequency pendulum and enables the theoretical detection of millihertz gravitational waves.

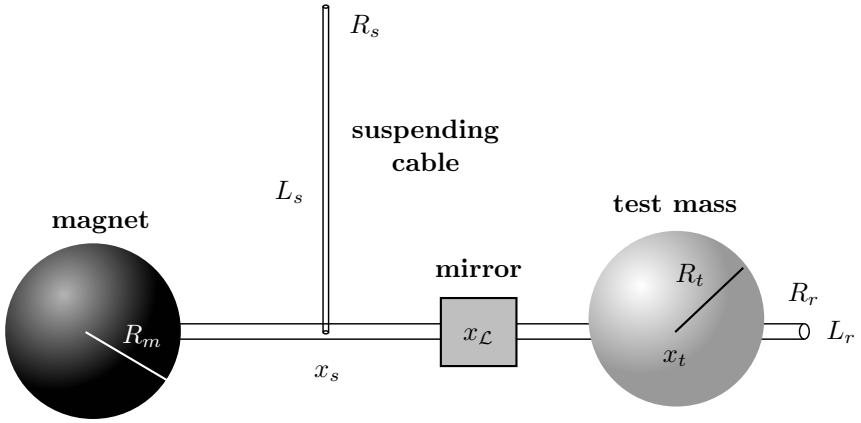

Figure 4: Illustration of the magnetically assisted gravitational-wave pendulum intorsion. The same cartesian and rotational axes are adopted as those in Figure 3. A spherical magnet of radius R_m, mass m_m and remanence $B_m\hat{\boldsymbol{z}}$ is fixed at the left end of the torsion pendulum arm ($x = 0$, when the arm is parallel to the ground). The arm is suspended at x_s by a cable of radius R_s and length L_s, made of material with modulus of rigidity G_s and yield strength σ_y. A mirror of negligible weight is fixed at the 'Levin point' $x_{\mathcal{L}}$, though this is not a free parameter. A spherical test mass of mass m_t and radius R_t is positioned at x_t. The pendulum arm is supported by a cylindrical rod of length L_r, radius R_r and mass m_r.

3 Background Theory

3.1 Gravitational Wave Coupling

An incident gravitational wave of frequency f on a Michelson interferometer arm of length L induces a sinusoidal strain $h(t)$ of equal frequency [3]. This results in an apparent interferometer arm length $Lh(t)$, with second derivative $L\ddot{h}(t)$, causing an oscillatory change in the distance between free bodies in the plane orthogonal to the wave. If masses in the plane appear free (which, for pendulums, depends on the frequency of the wave), their displacements from their equilibrium positions is measurable and the wave detectable. Such motion of the test masses can be modelled as that resulting from a hypothetical driving force in constant, strain-free space, given by Newton's second law as

$$F(t) = mL\ddot{h}(t). \tag{1}$$

Since current gravitational wave observatories expect strains smaller than 1×10^{-21} [6], a small angle approximation is valid for pendulum test masses and allows us to assume this driving force always acts orthogonally to the arm of the pendulum across the pendulum's experienced range of motion.

3.2 Pendulums

The common pendulum is a simple suspension of a mass from a pivot with a swinging or rotational degree of freedom. Despite its simplicity, the mass's emulation of a free body in response to small displacements (in certain directions) makes it instrumental in the detection of gravitational waves.

We investigate the use of a torsion pendulum - one which employs a torsion restoring force - to replace linear pendulums in the detection of gravitational waves.

3.2.1 Seismic Noise

Terrestrial pendulums suffer notable seismic noise. Seismic vibration pervades across a broad band, introducing vibration at the upper suspension point (the pivot) of any terrestrially suspended pendulum. Though particular frequency bands of vibration are attributable to different sources, such as earthquake or human traffic and construction, the lack of fixity of the Earth's surface renders complete isolation, particularly at low frequencies, impossible.

Suppression of seismic noise is difficult, as is distinguishing it from a potential gravitational wave signal. The presence of seismic noise obfuscates any gravitational wave signal of similar frequency, hence why observation of gravitational waves of frequencies in the noise band to which the pendulum strongly responds, is unreliable.

3.2.2 Linear Pendulums

The well known resonant frequency f_0 of a linear pendulum, when fixed at a particular region on the Earth (of unchanging gravitational field strength), is modulated only through change in the length of the pendulum arm L [7].

$$f_0 = \frac{1}{2\pi}\sqrt{\frac{g}{L}}. \tag{2}$$

An oscillatory system's response to cyclic perturbation, such as a pendulum under the influence of seismic noise or a gravitational wave, is described by the system's *transfer function* [8]. The transfer function relates the frequency of a system's input to the amplitude of the system's stable oscillatory response of that frequency (after an infinite time, where initial conditions are transient).

The transfer function of a linear pendulum responding to an incident gravitational wave (modelled as oscillatory displacement due to Equation 1) is presented in 5a and derived from the equation of motion of a center-of-mass driven pendulum in Appendices A and B. Also presented in the linear pendulum's response to seismic noise (Figure 5b), as derived in Appendices C and D.

Figure 5a shows that above the resonant frequency, the test mass of a linear pendulum responds to horizontal perturbations as if it were (approximately) free, particularly over small displacements. Below the resonant frequency, the transfer function exponentially decays, and the test mass behaves as if it were rigidly fixed. Meanwhile, Figure 5b shows linear pendulums respond strongly to seismic noise below their resonant frequency, at which seismic noise is likely to occur due to its very wide

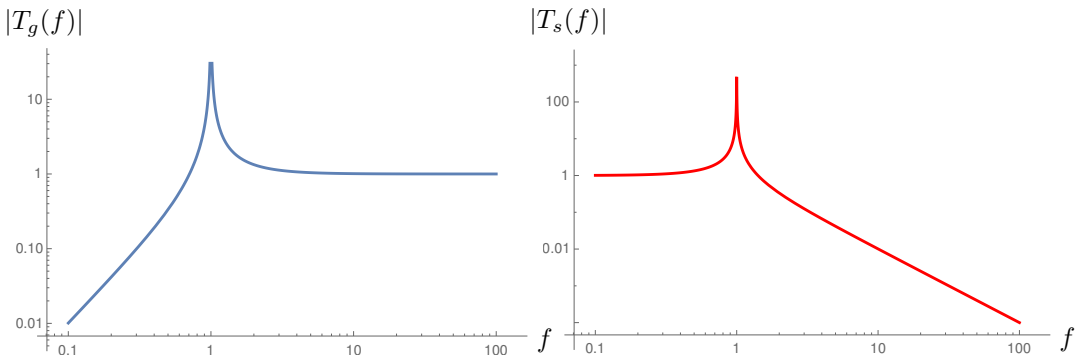

(a) Gravitational wave (frequency f) coupling of the linear pendulum.

(b) Response of the linear pendulum to seismic noise at frequency f.

Figure 5: Transfer functions of a linear pendulum of resonant frequency $f_0 = 1\,\text{Hz}$ in response to cyclic displacement at the test mass (blue) and the suspension point (red). These correspond to the system's oscillatory response to incident gravitational waves of frequency f and that to seismic noise (which acts at effectively all f) respectively. The blue curve shows good gravitational wave coupling above the resonant frequency but attenuation below, whilst the red curve shows that the linear pendulum is sensitive seismic noise of sub-resonant frequencies.

band. This indicates linear pendulums are practical only for the detection of gravitational waves of frequency above the pendulum's resonant frequency.

Because the resonant frequency goes like $f_0 \sim \frac{1}{\sqrt{L}}$, its reduction by increase in pendulum arm length is unfeasible, requiring huge increases in the height of the pendulum supporting structures.

3.2.3 Torsion Pendulums

Whereas linear pendulums feature rigid suspending arms, torsion pendulums are suspended with cables which may twist, with a 'rotational stiffness' k depending on the material of the cable. This allows the pendulum to yaw (see Figure 3), about which the resonant frequency depends on both k and the moment of inertia about the suspension point I_s [7].

$$f_0 = \frac{1}{2\pi}\sqrt{\frac{k}{I_s}}. \tag{3}$$

The resonant frequency of a torsion pendulum is significantly easier to modulate than that of a linear pendulum. The length, radius and choice of material of the cable can be modified, or the location, masses and sizes of the bodies along the pendulum adjusted to change k and I_s respectively.

TRANSFER FUNCTIONS

LEVIN POINT

COMPARE LINEAR TO TORSION

3.3 Permanent Magnets

3.3.1 Spherical

Due to the high symmetry, modelling the magnetic dipole and magnetic field of a spherical magnet is significantly easier than for other natural magnet geometries, such as cylindrical.

The magnetic moment of a spherical magnet of radius a and uniform permanent magnetization $\boldsymbol{M}$ is

$$\boldsymbol{\mu} = \frac{4\pi a^3}{3}\boldsymbol{M} \tag{4}$$

where the relationship between magnetization and internal magnetic field $\boldsymbol{B}_{\text{in}}$ (the remanent magnetization for a ferrimagnet) is

$$\boldsymbol{B}_{\text{in}} = \frac{8\pi}{3}\boldsymbol{M}, \tag{5}$$

noting the use of Gaussian units [9, p. 195].

This suggests, by also substituting $\boldsymbol{B}_{\text{in}} \to \sqrt{\frac{4\pi}{\mu_0}}\boldsymbol{B}_{\text{in}}$ and $\boldsymbol{\mu} \to \sqrt{\frac{\mu_0}{4\pi}}\boldsymbol{\mu}$, that the magnetic dipole moment is given in terms of the internal magnetic field (both now in the MKS system of units) as

$$\boldsymbol{\mu} = \frac{2\pi a^3}{\mu_0}\boldsymbol{B}_{\text{in}}. \tag{6}$$

The uniformly magnetized sphere is a perfect magnetic dipole; its fields are dipole in characteristic even at close proximity [9, p. 195], allowing calculation of its external magnetic field by that of a magnetic dipole.

$$\boldsymbol{B}(\boldsymbol{r}) = \frac{\mu_0}{4\pi}\left(-\frac{\boldsymbol{\mu}}{|\boldsymbol{r}|^3} + 3\frac{(\boldsymbol{\mu}\cdot\boldsymbol{r})}{|\boldsymbol{r}|^5}\boldsymbol{r}\right) \tag{7}$$

$$= \frac{a^3}{2}\left(-\frac{\boldsymbol{B}_{\text{in}}}{|\boldsymbol{r}|^3} + \frac{3(\boldsymbol{B}_{\text{in}}\cdot\boldsymbol{r})}{|\boldsymbol{r}|^5}\boldsymbol{r}\right). \tag{8}$$

A point at a distance x from the magnet's centre along a line parallel to the remanent magnetization (let $\boldsymbol{B}_{\text{in}} = B_{\text{in}}\hat{\boldsymbol{x}}$ and $\boldsymbol{r} = x\hat{\boldsymbol{x}}$) will thus experience a magnetic field of

$$\boldsymbol{B}(x\hat{\boldsymbol{x}}) = \frac{a^3}{x^3}B_{\text{in}}\hat{\boldsymbol{x}}.$$

3.3.2 Cylindrical

Although retaining azimuthal symmetry, a cylindrical magnet (of uniform magnetization parallel to its axis) does not perfectly resemble a dipole and its magnetic field must be found by volume integration. Although the field may be analytically found along the cylindrical axis [10], its general calculation at arbitrary points in space are more easily performed numerically [11].

We're particularly interested in the homogeneity of the external magnetic field along the boundaries of the suspended magnet when placed in the field of the external magnet.

The magnetic field along the z-axis (beginning at a circular face where the other face is encountered for positive z) of a cylindrical magnet of height L and radius R with uniform internal magnetic field $\boldsymbol{B}_{\text{in}}$ (parallel to the cylindrical axis) is

$$\boldsymbol{B}(z) = \frac{\boldsymbol{B}_{\text{in}}}{2}\left(\frac{z}{\sqrt{z^2+R^2}} - \frac{z-L}{\sqrt{(z-L)^2+R^2}}\right) \quad [10]$$

WAT was I going to do here??

4 Torsion Pendulum Configuration

The pendulum arm of the MAGPI design is illustrated in Figure 4. It features a spherical test mass attached to a cylindrical rod, countered by an attached spherical, permanent magnet which interacts with an external magnetic field. A cylindrical cable suspends the rod from a fixed upper suspension point.

The critical challenge of a small-scale implementation of the MAGPI design is the configuration of its large number of inter-dependent physical parameters. The physical parameters related only to the arm and cable of the pendulum are compiled in Table 1.

A valid configuration must see the gravitational and magnetic torques on the pendulum balance, yield a center of mass suitably apart from the suspension point and a Levin point which lies within the bounds of the arm, achieve a yaw resonant frequency in the millihertz band, feature a suitably strong cable to suspend the pendulum arm and require an external magnet field of achievable strength (the generation of which presents another set of parameters and constraints).

Although the tasks of constructing an appropriately sized table-top torsion pendulum and generating an external magnetic field sufficient to suspend it appear separate, the delicate interplay between the pendulum's size and mass distribution, the parameters of the field's generator and its introduction of additional noise in the pendulum, require the tasks are carefully and simultaneously performed.

4.1 Center of Mass

Let the x-axis span the length of the pendulum arm from left to right, fixing the lower suspension point at x_s, the magnet at $x = 0$ and the test mass at x_t (see Figure 4). Assume the arm constituted by some cylindrically symmetric rod of length L_r and mass m_r. Assign also the magnet a mass of m_m and the test mass m_t, giving the pendulum arm a total mass of

$$M = m_m + m_r + m_t. \quad (9)$$

The center of mass x_c of the pendulum is confined along this x-axis (between 0 and L_r), at

$$x_c = \frac{1}{M}\left(m_r\frac{L_r}{2} + m_t x_t\right). \quad (10)$$

Symbol	Unit	Description
R_r	m	Radius of the supporting cylindrical rod
L_r	m	Length of the rod
m_r	kg	Mass of the rod
R_s	m	Radius of the suspending cylindrical cable
L_s	m	Length of the cable
x_s	m	Position of the suspension point along the pendulum arm
G_s	Pa	Modulus of rigidity of the cable
σ_y	Pa	Yield strength of the cable
R_m	m	Radius of the attached (at $x = 0$) spherical magnet
m_m	kg	Mass of the magnet
B_m	T	Remanence of the magnet
R_t	m	Radius of the attached spherical test mass
x_t	kg	Position of the test mass
m_t	kg	Mass of the spherical test mass

(a) Physically configurable parameters.

Symbol	Unit	Description
M	kg	Total mass of the pendulum arm
x_c	m	Center of mass of the pendulum arm, along the length of the arm
I_c	$\mathrm{kg\,m^2}$	Moment of inertia (yaw & pitch) about the center of mass of the arm
k_s	$\mathrm{N\,m\,rad^{-1}}$	Rotational stiffness of the suspending cable
I_s	$\mathrm{kg\,m^2}$	Moment of inertia (yaw & pitch) about the suspension point
f_0	Hz	Resonant frequency of the pendulum about the yaw axis
$x_{\mathcal{L}}$	m	Levin point of the pendulum arm
τ_g	N m	Gravitational torque on the pendulum arm about the suspension point
μ_m	$\mathrm{N\,m\,T^{-1}}$	Magnetic dipole moment of the attached magnet

(b) Resulting quantities.

Table 1: Physical parameters and resulting quantities of the pendulum arm. The use of an above symbol starred indicates that quantity when the system is constrained by having a suspension point and test mass at opposite ends of the rod and a test mass and magnet of equal mass and radius.

When the test mass is fixed at the end of the pendulum arm ($x_t = L_r$) and has the same mass as the attached magnet ($m_m = m_t$), the center of mass simplifies to

$$x_c' = \frac{L}{2}. \tag{11}$$

Such a circumstance is motivated in Section 4.3.1.

4.2 Moment of Inertia

The moment of inertia of the pendulum for yaw and roll about both its center of mass x_c and the suspension point x_s is required for calculation of the Levin point, the pendulum's resonant frequency and the magnitude of extraneous torques.

Exploiting that moment of inertia is additive, we can combine that of each constituent of the pendulum arm (the rod, magnet and test mass) about the center of mass, translated there from their own natural rotational axis by the parallel axis theorem.

Consider first the spherical magnet of radius R_m attached to the left end of the rod with a mass m_m, distributed uniformly as is characteristic of permanent magnets. CIIIIIIIITE THIIISSSS. Translating its moment of inertia about its diameter [12] at $x = 0$ to that about the center of mass of the pendulum arm by the parallel axis theorem [13] yields

$$I_m = \frac{2}{5} m_m {R_m}^2 + m_m {x_c}^2. \tag{12}$$

The moment of inertia of the spherical test mass is calculated similarly, though is translated from its position at x_t.

$$I_t = \frac{2}{5} m_t {R_t}^2 + m_t \left(x_t - x_c\right)^2. \tag{13}$$

These fixtures are attached to the cylindrical rod of radius R_r, length L_r and uniformly distributed mass m_r, which is considered rotating about its central diameter [12] before translation to the center of mass by the parallel axis theorem.

$$I_r = \frac{1}{12} m_r {L_r}^2 + \frac{1}{4} m_r {R_r}^2 + m_r \left(\frac{L_r}{2} - x_c\right)^2. \tag{14}$$

The moment of inertia of the pendulum arm for yaw and roll about its center of mass is then the sum of Equations 12, 13 and 14.

$$I_c = I_m + I_t + I_r. \tag{15}$$

The moment of inertia for similar rotations about the suspension point x_s is found by the parallel axis theorem [13] to be

$$I_s = I_c + M(x_c - x_s)^2. \tag{16}$$

For the particular setup (proposed in Section 4.3.1) where the test mass is fixed at the end of the rod ($x_t = L_r$) and has an equal mass and radius as the attached magnet ($m_t = m_m$, $R_t = R_m$) which is fixed at the suspension point ($x_s = 0$), the moments of inertia simplify to

$$I_c^* = \frac{1}{60}\left(5{L_r}^2(6m_m + m_r) + 48m_m{R_m}^2 + 15m_r{R_r}^2\right) \tag{17}$$

and

$$I_s^* = {L_r}^2\left(m_m + \frac{m_r}{3}\right) + \frac{4}{5}m_m{R_m}^2 + \frac{1}{4}m_r{R_r}^2. \tag{18}$$

4.3 Levin Point

INTRODUCE CONCEPT OF SWEET-SPOT: SHOW TRANSFER FUNCTION CHANGE. Maybe don't do this here????? Put in bakcground theory!

The Levin point occurs at a distance along the pendulum arm [14]

$$x_{\mathcal{L}} = \left(1 + \frac{m_t{x_c}^2}{I_c}\right)x_c. \tag{19}$$

Notice this is not bound within $[0, L_r]$ and through the presence of the center of mass (Equation 10) and the moment of inertia for yaw about the arm's center of mass (Equation 16) REFERENCE TO THIS EQUATION WHEN YOU MAKE IT, presents a complicated relationship with the other parameters of the pendulum. SHOW HOW BAD IT REALLY IS

Numerical calculation for a variety of hypothetical (order of magnitude) pendulum configurations demonstrated difficulty in achieving a Levin point confined to the length of the pendulum arm (i.e. $x_{\mathcal{L}} \leq L$), particularly when mass was concentrated around the center of mass. Though of the right order of magnitude, the Yuri point appeared several times the length of the pendulum arm past the center of mass, when the center of mass was closer to the test mass.

Pushing the test mass closer to the suspension point requires caution, since this reduces the measurable response of the pendulum to gravitational coupling.

4.3.1 Analytic Approximation

To guide numerical investigation, we establish a simpler model to approximate our setup, where the spherical magnet shares mass and radius with the test mass; m and r respectively. Note that raising the mass of the attached magnet disturbs the equilibrium between gravitational and magnetic torque on the pendulum but not harmfully; it reduces the required magnetic torque. Raising the arm's total mass however demands greater strength of the suspending cable and perturbs the resonant yaw frequency of the pendulum. Assume that the rod is of negligable mass and does not contribute to the moment of inertia.

Fixing the test mass at x_t presents a center of mass

$$x_c^* = \frac{x_t}{2} \tag{20}$$

with a moment of inerta found by adding those due to each of the magnet and test mass (as spinning spheres [12]), translated to the center of mass by the parallel axis theorem CITE THE PARALLEL AXIS THEOREM.

$$I_c^* = m\left(\frac{4}{5}r^2 + \frac{{x_t}^2}{2}\right). \tag{21}$$

Such a system presents a Levin point, independent of mass, at

$$x_{\mathcal{L}}^* = \frac{x_t}{4}\left(2 + \frac{5{x_t}^2}{8r^2 + 5{x_t}^2}\right). \tag{22}$$

Equation 22 is remarkably linear in both low and high limits of x_t, and shows negligable functional variation across r in the $[1\,\text{mm}, 10\,\text{cm}]$ (the extremities of feasible magnet size). Notice

$$x_{\mathcal{L}}^*|_{r=0} = \frac{3}{4}x_t \qquad \text{meanwhile} \qquad \lim_{r\to\infty} x_{\mathcal{L}}^* = \frac{1}{2}x_t, \tag{23}$$

suggesting the Levin point as a fraction of the arm length is bounded within

$$\frac{x_{\mathcal{L}}^*}{x_t} \in \left[\frac{1}{2}, \frac{3}{4}\right] \tag{24}$$

for all positions of the test mass and equal radii of the magnet and test mass.

We now relax our approximation by introducing the moment of inertia of the rod into the Levin point, positioning the test mass at the end of the rod ($x_t = L_r$) and maintaining the equal mass and radii of the test mass and attached magnet (denoting them m_t and R_t respectively). The rod's moment of inertia is that of a cylinder rotating about its center diameter (and center of mass) [12].

$$I_{\text{r}}^* = \frac{1}{12}m_r{L_r}^2 + \frac{1}{4}m_r{R_r}^2. \tag{25}$$

Equation 19 indicates an increase in the moment of inertia (as the introduction of the rod incurs) brings the Levin point closer to the center of mass. There is thus no concern of our rod translating the Levin point to beyond the bounds of the pendulum arm.

We happily remark also that it perturbs the Levin point toward the center of mass negligably. Substituting the mass of the rod as a fraction α of the test mass ($m_r = \alpha m_t$) presents a Levin point as a fraction of the rod length

$$\frac{x_{\mathcal{L}}^*}{L_r} = \frac{1}{2} + \frac{15{L_r}^2}{(6+\alpha)10{L_r}^2 + 96{R_t}^2 + 30{R_r}^2}. \tag{26}$$

Allowing α to vary between extremities $\alpha \in [0, 1]$ (corresponding to a massless rod or one as heavy as the test mass) negligably affects the location of the Levin point. This is realised by substituting $R_t = R_r = 0$ into Equation 26 (whereby variation in α becomes most significant) and observing a variation in the position of the Levin point of only 6% the length of the rod.

We're now assured that regardless of the particular physical values, a pendulum configuration which features the test mass fixed at the end of the rod, equal in mass and radius with the magnet, will

support a Levin point within the bounds of the pendulum arm, between halfway and three-quarters the length of the arm. This will be adopted as a constraint, though only for configurations where the suspension point is not the midpoint between the magnet and test mass, otherwise the center of mass is at the yaw axis and gravitational-wave coupling is impossible.

$$\begin{cases} m_m = m_t, \\ R_m = R_t \end{cases} \implies x_{\mathcal{L}} \in [0.5, 0.75] L_r. \tag{27}$$

4.4 Suspending Cable

The resonant frequency of the torsion pendulum (Equation 3) depends both on the moment of inertia about the suspension point I_s and the rotational stiffness k_s of the suspending cable. For simplicity, we'll model the cable as cylindrical, made from a continuous, linearly elastic material, where rotational strain is linearly dependent on rotational stress, constituted by local, infinitesimal shear stresses [15]. The cable with circular cross-section is depicted in Figure 6.

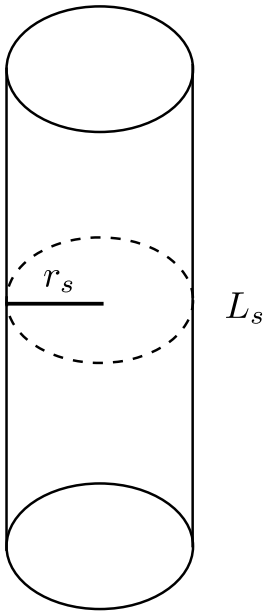

Figure 6: Illustration of the suspended cable with exaggerated radius

The rotational stiffness depends on the length L_s and radius r_s of the cable and its modulus of rigidity (or *shear modulus*) G_s; a property of the cable's material which measures responding strain to shear stress. The relationship [16] is derived in Appendix G.

$$k_s = \frac{G_s \pi {r_s}^4}{2 L_s}. \tag{28}$$

This, with Equation 3, constrains the suspending cable length with its radius in order to achieve a particular resonant frequency for a given torsion pendulum arm configuration (encapsulated in the yaw moment of inertia I_s).

$$L_s = \frac{G_s {R_s}^4}{8 \pi {f_0}^2 I_s}. \tag{29}$$

This is highly sensitive to the radius; small increases in radius yield drastic increases in the required length of the suspending cable, otherwise incuring a quadratic change in resonant frequency ($f_0 \sim \frac{{R_s}^2}{\sqrt{L_s I_s}}$). When constructing a small-scale MAGPI, an appreciable surplus of suspending cable should be purchased, and the radius of the cable should be kept economically low.

However, we note with caution that the finite strength of the suspending cable fixes a lower limit on the radius. The weight of the pendulum arm exerts a pressure across the cross-section of the cable, which should be kept significantly lower than the yield strength σ_y of the cable material.

$$\frac{F}{A} = \frac{Mg}{\pi {R_s}^2} \ll \sigma_y. \tag{30}$$

If the pressure exceeds the yield strength, the cable may be inelastically deformed and if the pressure is not kept an order of magnitude smaller, elastic extension of the cable will disturb the resonant frequency.

KEEP GOING

4.5 Gravitational Torque

Gravity exerts a downward force at the pendulum's center of mass, which depends on the pendulum's total mass M and the acceleration of bodies near the Earth's surface g. It therefore delivers a torque [17] about the suspension point of

$$\boldsymbol{\tau}_g = (x_c - x_s)\hat{\boldsymbol{x}} \times (-Mg)\hat{\boldsymbol{z}} \tag{31}$$

$$= Mg(x_c - x_s)\hat{\boldsymbol{y}}, \tag{32}$$

which would see clockwise rolling in Figure REFERENCE TO THE ROTATIONS FIGURE HERE!!.

Static equilibrium of the pendulum about the roll axis requires this gravitational torque be opposed by an equal magnetic torque, as produced by the interaction between the attached magnet and an external magnetic field.

5 External Magnetic Field Generation by Helmholtz Coils

5.1 Parameters

The earliest mini-MAGPI design iteration features a spherical, permanent magnet attached below the suspension point (at $x_s = 0$). With radius R_m and upward (vertically) pointing, uniform, internal magnetisation $\boldsymbol{B}_{\text{in}} = B_m\hat{\boldsymbol{z}}$, the magnet's magnetic dipole moment is calculated through Equation 6 to be

$$\boldsymbol{\mu}_m = \frac{2\pi}{\mu_0} {R_m}^3 B_m \hat{\boldsymbol{z}}. \tag{33}$$

A left pointing, homogeneous, external magnetic field $\boldsymbol{B}_e(\boldsymbol{r}) = -B_e(\boldsymbol{r})\hat{\boldsymbol{x}}$ must be of sufficient magnetic field strength B_e at the region of the attached magnet so as to produce a magnetic torque $\boldsymbol{\tau}_m$ [17] to counter the gravitational torque.

$$\boldsymbol{\tau}_m = \boldsymbol{\mu}_m \times \boldsymbol{B}_e \tag{34}$$

$$= -\frac{2\pi}{\mu_0} {R_m}^3 B_m B_e \hat{\boldsymbol{y}}. \tag{35}$$

Imposing the torques balance (Equation 32 with Equation 35) presents a required external magnetic field strength.

$$B_e = \frac{\mu_0 g}{2\pi} \frac{Mx_c}{B_m {R_m}^3}. \tag{36}$$

Symbol	Unit	Description
R_H	m	Radius and separation of the Helmholtz loops
N_H		Number of windings of wire around each loop
J_H	A	Current through the loops
R_w	m	Radius of the wire wound around each loop
ρ_w	Wm	Resistivity of the wound wires
α_w	m/m K	Coefficient of linear thermal expansion of the wire material
ϵ_H		Emissivity of the Helmholtz loops
η		Packing density of wires in Helmholtz loop bundle

(a) Physically configurable (though not all tunable) parameters.

Symbol	Unit	Description
R_b	m	Cross-sectional radius of the wire bundle of each loop
S_b	m^2	Total exterior surface area of both wire bundles (combined)
L_w	m	Total length of wound wire (between both loops)
ζ_H	Ω	Total electrical resistance of both coils (combined)
P_H	W	Total power dissipated between both coils (combined)
T_H	K	Equilibrium (radiative) temperature of the Helmholtz coil

(b) Resulting quantities.

Table 2: Physical parameters and resulting quantities of the Helmholtz coil.

The intuitive device for the controlled generation of magnetic fields in a laboratory environment is the Helmholtz coil. When the magnetic coils of N_H windings and radius R_H are separated by R_H, a current J_H through the coils produces a magnetic field at the center of the coil pair of strength [17]

$$B_H = \frac{8}{5\sqrt{5}} \frac{\mu_0 N_H J_H}{R_H}. \tag{37}$$

The available, configurable parameters of the Helmholtz coils and the resulting physical quantities are compiled in Table 2.

The magnetic field produced by a Helmholtz coil is very homogeneous along the axis of symmetry, but less so off-axis, where the field grows weaker [17]. Precise calculation of the magnetic torque on the attached magnet requires calculation of the external magnetic field strength at all points in the space occupied by the attached magnet. Modeling the magnetic field off-axis is difficult and unnecessary; instead, the field will be assumed homogenous everywhere between the coils, of strength equal to that at the center. This will present an insignificant underestimate of the required external field strength, still useful for judging the feasibility of field generation with a Helmholtz coil.

We remark that construction of a mini-MAGPI experiment does not require precise knowledge of the external field strength. Instead, the field strength may be modulated by control of the current in the coil, to experimentally achieve a balanced pendulum arm.

Attempting to generate our external field with a Helmholz coil and equating Equations 36 and 37

constraints the pendulum arm parameters with the Helmholtz coil parameters.

$$J_H = \frac{5\sqrt{5}g}{16\pi} \frac{Mx_c}{B_m {R_m}^3} \frac{R_H}{N_H}. \tag{38}$$

If we introduce the simplifying assumption that the test mass and attached magnet have equal mass and radius (as motivated in Section 4.3.1), we can express the required Helmholtz current in terms of the rod length L_r, rod mass m_r, magnet (and test mass) mass m_m and radius of the attached magnet (and test mass) R_m (substituting Equation 11).

$${J_H}^* = \frac{5\sqrt{5}g}{32\pi} \frac{L_r(2m_m + m_r)}{B_m {R_m}^3} \frac{R_H}{N_H}. \tag{39}$$

I DON'T WANT TO APPLY SIMPLIFYING ASSUMPTIONS YET! I CHANGED MY MIND

This is formulated for current which is easier to modulate (may be stepped up or down with transformers) than physical parameters like the number of turns and the radius of the loops.

Equation 39 goes like $J_H \sim {R_m}^{-3}$ and is very sensitive to changes in radius of our attached magnet. This is no surprise since volume also goes like the cube, suggesting

$$J_H \sim \frac{1}{V_m}, \tag{40}$$

where V_m is the volume of the attached (spherical) magnet. We caution however that the radius of the attached magnet must be considered in conjuction with the separation of the Helmholtz coils, within which the magnet must fit. The mass of the magnet m_m also varies with the cube of its radius ($m_m \sim {R_m}^3$) if a particular magnetic material is chosen.

This actually gives appreciably low currents! Like 12V for 200 turns and 2cm radius magnets! Yay!?

Should I estimate stuff here?!

5.2 Geometric Model

When the Helmholtz coil is operational, our desirably static pendulum arm suggests no power is disspated in the produced magnetic field. All power is instead dissipated as heat through the wound wires which make the coils, and may require evacuation.

Recall that our required field strength is a small underestimate. Calculation of the power of the Helmholtz coil requires estimation of its total electrical resistance, which in turn necessitates a more precise geometric model of the loops.

We model the wire bundle of each loop as a torus; a closed loop of circular cross-section. This is an acceptable approximation which ignores the insignificant irregularity at the bundle surface (which is not smooth) and at the end-points of the wire (which are connected to positive and negative terminals).

The wires are assumed, when laid flat, cylindrical with radius R_w. We can approximate the total length of wire required (expected as a small underestimate) as that of N_H rings of radius R_H, for each loop. This suggests a total length (of both loops combined) of

$$L_w = 4\pi N_H R_H, \tag{41}$$

with circular cross-sectional area

$$A_w = \pi {R_w}^2. \tag{42}$$

Assigning our wires resistivity ρ_w, Equations 41 and 42 suggest a total electrical resistance [18] in our Helmholtz coils of

$$\zeta_H = 4\rho_w \frac{N_H R_H}{{R_w}^2}. \tag{43}$$

We'll here continue our geometric description of the Helmholtz coil, used in subsequent calculations. To estimate the total exterior surface area of our wire bundle, we must first estimate its circular cross-sectional radius, based on the packing of N_H instances of radius R_w wire cross-sections (circles) into said cross-section.

The total cross-sectional area of torus, required to fit N_H instances of wire, is related to the total cross-sectional area of wire by a circular packing density $\eta \in (0, 1]$. The wire bundle's cross-sectional radius can be related back to this packing density as

$$R_b = R_w \sqrt{\frac{N_H}{\eta}}, \tag{44}$$

and, together with the radius of our Helmholtz coils, suggests a total exterior surface area [19] of *both* the torus wire bundles (combined) of

$$S_b = 8\pi^2 R_w R_H \sqrt{\frac{N_H}{\eta}}. \tag{45}$$

DIAGRAMSSSSS OF TORUSSSSSS AND OF CROSS-SECTION!!!!!!

5.3 Heat Generation

The total power generated by both Helmholtz coils, output as heat through the wire bundles, can now be approximated as (substituting Equations 38 and 43)

$$P_H = {J_H}^2 \zeta_H \tag{46}$$

$$= \frac{\rho_w}{N_H} \left(\frac{gMx_c}{\pi B_m R_w} \right)^2 \left(\frac{5}{4} \frac{R_H}{{R_m}^2} \right)^3. \tag{47}$$

This is not the net power into the coils, which may also absorb heat from its environment by radiation and convection.

SHOULD WE CALCULATE THE POWER GENERATED NUMERICALLY HERE? IF YOU DON'T USE SIMPLIFYING ASSUMPTIONS, YOU MUST DISCLAIM THAT THE LEVIN POINT MAY BE INCONVENIENT (OFF THE BAR)

5.4 Heat Evacuation by Radiation

Ideal circumstances would see all generated heat effectively evacuated from the Helmholtz coil by thermal radiation. This is preferential, since containment of the small-scale MAGPI setup inside a vacuum chamber makes other methods of evacuation challening. The Stefan-Boltzmann law [20] gives the power of thermal radiation of our Helmholtz coil, when the coils (of emissivity ϵ_H) are at temperature T'_H, as

$$P'_H = \sigma \epsilon_H S_b {T'_H}^4, \tag{48}$$

where σ is the Stefan-Boltzmann constant ($\sigma \approx 5.67 \times 10^{-8}\,\mathrm{W\,m^{-2}\,K^{-4}}$).

Comparison with Equation 47 (and substitution of Equation 45) presents an underestimate of the temperature T_H of the coils at which all generated heat is effectively radiated.

$$T_H \approx \frac{1}{4\pi} \left(\frac{g M R_H x_c}{B_m {R_m}^3} \right)^{1/2} \left(\frac{5^3}{2} \frac{\rho_w}{\sigma \epsilon_H {R_w}^3} \right)^{1/4} \left(\frac{\eta}{{N_H}^3} \right)^{1/8}. \tag{49}$$

This ignores the additional, extraneous source of heat by thermal absorption from the environment, which would see a higher temperature of equilibrium, though is sufficient for assessing the feasiliby of radiative heat evacuation.

We can emulate a black body by painting our wires black and setting $\epsilon_H \approx 1$ [20]. The feasibility of radiative cooling is judged by the magnitude of T_H; whether it is appropriately cool for operation in a laboratory environment, to be sustained well below temperatures which would incur melting or deformation of the setup. A reasonable threshold was assumed to be $T \approx 100\,^\circ\mathrm{C}$ (the boil point of water), beyond which we expect our paint to melt or evaporate and our Helmholtz wires to expand appreciably ($\sim 10^0\,\mathrm{mm}$).

Uniform, linear thermal expansion $\Delta L_w = \alpha_w L_w \Delta T$ [21] of the Helmholtz coil wires sees an increase in the radius of (approximately) each winding (and thus the approximate Helmholtz loop radius) of

$$\Delta R_H = \frac{\alpha_w L_w \Delta T}{2\pi N_H}, \tag{50}$$

where α_w is the linear thermal coefficient of the wire, specific to its material. Taking $\Delta T = T_H - 293$ (the difference in the equilibrium temperature and room temperature) allows calculation of the expansion of the Helmholtz loop radius as the loops warm during operation.

Numerical estimates of the small-scale MAGPI parameters and their propogation to physical quantities are presented in Table 3, and present an underestimated minimum temperature of the Helmholtz coils to achieve stable radiative cooling of $T_H \approx 120\,^\circ\mathrm{C}$; above the acceptable threshold.

At a temperature of $T_H \approx 120\,^\circ\mathrm{C}$, the considered Helmholtz loop radii expand by 0.3 mm, or 0.3%. This is small, but unrealistically assumes each loop of wire expands concentrically. Instead, wire expansion of such magnitude is likely to altar the packing arrangement of the wires in the bundle, deforming the Helmholtz loops.

Since Equation 49 shows notable insensitivity to most parameters, reducing this temperature by careful parameter choice is difficult. Furthermore, the assumed parameters offered in Table 3 feature a center of mass quite close to the suspension point ($x_c = 10\,\mathrm{cm}$). Better gravitational-wave coupling occurs when the center of mass is further out, for which the gravitational torque increases

Symbol	Value	Unit	Description
M	1	kg	Total mass of the pendulum arm
x_c	10	cm	Center of mass of the pendulum arm
R_m	2	cm	Radius of the attached magnet
B_m	1	T	Remanence of the attached magnet (typical of ferromagnets [22])
R_H	8	cm	Radius of the Helmholtz coil
N_H	200		Number of turns of wire wrapped around each Helmholtz coil
R_w	1	mm	Radius of the wires of the Helmholtz coils
ρ_w	1.7×10^{-8}	$\Omega\,\mathrm{m}$	Electrical resistivity of the Helmholtz coil wires (that of Copper [23])
α_w	16.6×10^{-6}	$\mathrm{m/m\,K}$	Coefficient of linear thermal expansion of the Helmholtz coil wires (that of Copper [24])
η	0.8		Packing factor of the wires in the Helmholtz coil bundles [25]

(a) Assumed pendulum arm and Helmholtz coil parameters.

Symbol	Value	Unit	Description
P_H	130	W	Power generated by the Helmholtz coil (as heat)
T_H	390	K	Minimum temperature of the Helmholtz coils required to radiate all heat
B_H	25	mT	Magnetic field strength generated by the Helmholtz coils at their center
J_H	11	A	Current required through the Helmholtz coil
ΔR_H	0.3	mm	Expansion in Helmholtz coil radius incurred from room temperature to T_H.

(b) Relevant resulting quantities.

Table 3: Estimated numerical values of the small-scale MAGPI parameters and the relevant resulting physical quantities.

as does the required external field strength, and consequentially the power and temperature of the Helmholtz coils also go up.

The results in Table 3 demonstrate radiative cooling is insufficient and an active mechanism of heat evacuation from the Helmholtz coil must be employed.

5.5 Heat Evacuation by Convection

We also considered the cooling of the Helmholtz coils by convective heat transfer. With the small-scale MAGPI setup contained in a vacuum chamber, convective cooling requires the pumping of water through the system. An electrically insulating, thermally conductive material must separate the water and the coils to prevent short-circuit, and the pendulum arm cannot contact the coolant without experiencing severe mechanical noise due to fluid forces [26].

Pumping coolant through a tube which contacts only the Helmholtz coil loops still produces additional noise. Fluid turbulence would cause undirected vibration in the tube and Helmholtz loops [26]. Due to the inhomogeneity of the external magnetic field off the axis of symmetry, vibration of the loops lead to fluctuation of the magnetic field strength experienced by the attached magnet, and therefore the magnetic torque on the pendulum arm. Fluctuation in the net torque sees the pendulum arm destabilise and roll, introducing significant mechanical noise into the system.

There are therefore no obvious, acceptable, convective methods of heat evacuation from the Helmholtz coil.

5.6 Heat Evacuation by Conduction

Heat may also be conducted away from the Helmholtz coils to a cold reservoir. A thermal conductor can be in contact with (though electrically insulated from) the Helmholtz coils and connect to a simple ice bath kept at 0 ° by the ice to water phase change [27]. Replenishment of the ice in the bath can sustain the reservoir indeterminately, at conveniently infrequently as judged by the power of the coils in Table 3.

SHOULD I CALCULATE A FREQUENCY UPPERBOUND OF CHANGING ICE BASED ON ENTHALPY OF FUSION??

Fourier's law gives the rate of heat P_c conducted from the Helmholtz coils at temperature T_H through a medium of thermal conductivity κ_c, length L_c and area (at right angles to the heat gradient) A_c [28], to a 0 °C reservoir as

$$P = \kappa_c A_c \frac{T_H - 273}{L_c}. \tag{51}$$

[29] [30] [31]

5.7 Numerical Assessment

6 External Magnetic Field Generation by Ferrimagnets

6.1 Spherical

6.2 Cylindrical

6.3 Rings

6.3.1 Displacing Instability

6.3.2 Flip Instability

7 Other Considerations

- Thermal noise
- Eddy current noise
- Radiation noise

8 Conclusions

References

[1] "A comprehensive overview of advanced ligo," February 2015. Accessed: 09-11-2015.

[2] C. Cutler and K. S. Thorne, "An Overview of Gravitational-Wave Sources," Apr. 2002.

[3] C. Sopuerta, *Gravitational Wave Astrophysics: Proceedings of the Third Session of the Sant Cugat Forum on Astrophysics*. Astrophysics and Space Science Proceedings, Springer International Publishing, 2015.

[4] "Ligo fact sheet," October 2001. Accessed: 10-11-2015.

[5] J. Aasi *et al.*, "Advanced LIGO," *Class. Quant. Grav.*, vol. 32, p. 074001, 2015.

[6] A. B. P. e. a. Aasi J, Abadie J, "Enhanced sensitivity of the ligo gravitational wave detector by using squeezed states of light," *Nature Photonics*, no. 7, 613-619, 2013.

[7] J. C, *Textbook Of Engineering Physics*. No. pt. 1, Prentice-Hall Of India Pvt. Limited.

[8] R. Dorf and R. Bishop, *Modern Control Systems*. Pearson Prentice Hall, 2008.

[9] J. Jackson, *Classical electrodynamics*. Wiley, 1975.

[10] J. M. Camacho and V. Sosa, "Alternative method to calculate the magnetic field of permanent magnetis with azimuthal symmetry," *Revista Mexicana de Fisica*, vol. 59, 2013.

[11] S. M. Blinder, "Magnetic field of a cylindrical bar magnet," 2011. Accessed: 23-09-2015.

[12] R. Serway, *Physics for scientists & engineers*. No. v. 2 in Physics for Scientists & Engineers, Saunders College Pub., 1986.

[13] C. Reviews, *e-Study Guide for Multivariable Mathematics, textbook by Theodore Shifrin: Mathematics, Mathematics*. Cram101, 2012.

[14] R. A. L. T. Eric Thrane, Yuri Levin, "Terrestrial detection of millihertz gravitational waves with magnetically assisted torsion pendulums," *School of Physics and Astronomy, Monash University, Clayton, Victoria, Australia*, 2015.

[15] N. H. Scott, "solid mechanics: Linear elasticity," *School of Mathematics, University of East Anglia, Norwich, NR4 7TJ, United Kingdom*.

[16] S. Gupta, *Engineering Physics: Vol. 1*. Krishna Prakashan.

[17] R. Serway, *Physics for scientists & engineers*. No. v. 2 in Physics for Scientists & Engineers, Saunders College Pub., 1986.

[18] C. Reviews, *e-Study Guide for Industrial Electricity, textbook by Michael E. Brumbach: Engineering, Electrical engineering*. Cram101, 2012.

[19] R. Schwartz, *Mostly Surfaces*. Student mathematical library, American Mathematical Society, 2011.

[20] J. Lienhard, *A heat transfer textbook*. Prentice Hall PTR, 1981.

[21] P. Shesha and G. S, *Textbook of Mechanics of Materials*. PHI Learning Pvt. Ltd.

[22] H. Meyers and H. Myers, *Introductory Solid State Physics, Second Edition*. Taylor & Francis, 1997.

[23] "Resistivity, conductivity and temperature coefficients for some common materials." Accessed: 2015-11-18.

[24] "Coefficients of linear thermal expansion." Accessed: 2015-11-18.

[25] S. E., "The best known packings of equal circles in a circle (complete up to n=2600)." http://hydra.nat.uni-magdeburg.de/packing/cci/, 2015. Accessed: 2015-11-18.

[26] A. MOHANTY, *FLUID MECHANICS*. PHI Learning, 1994.

[27] C. Reviews, *e-Study Guide for Chemistry: The Central Science, textbook by Theodore E. Brown: Chemistry, Chemistry*. Cram101, 2012.

[28] J. Fourier and A. Freeman, *The Analytical Theory of Heat*. The University Press, 1878.

[29] W. v. M. E. A. Burgemeister and E. Pettenpaul, "Thermal conductivity and electrical properties of 6h silicon carbide," *Journal of Applied Physics*, vol. 50, 1979.

[30] D. Lide, *CRC Handbook of Chemistry and Physics, 84th Edition*. CRC HANDBOOK OF CHEMISTRY AND PHYSICS, Taylor & Francis, 2003.

[31] "Water - thermal properties, the engineering toolbox." http://www.engineeringtoolbox.com/water-thermal-properties-d_162.html. Accessed: 15-09-2015.

[32] F. L. D.J. Dal Bello, S.a. Waltner, "Strength and stiffness of engineering systems," 2006. Accessed: 14-11-2015.

A Linear Pendulum Gravitational Coupling Equation of Motion

Consider a frictionless, linear pendulum of mass m and arm length l which swings in the x direction, in an interferometer of path-length L. Let $\theta(t)$ be the pendulum's angle with the vertical and $x_b(t)$ the horizontal position of the mass (with $x_b = 0$ below suspension), related exactly by $x_b = l\sin(\theta)$.

We can model a gravitational-wave strain as an oscillatory, extraneous force acting at the pendulum's center of mass. Assuming the strain is small, a small angle approximation enables us to assume this force always acts orthogonally to the arm of the pendulum, in the x-vertical plane.

We construct the vector-position and scalar-speed of the pendulum's mass.

$$\begin{aligned}\boldsymbol{x}(t) &= \big(l\sin(\theta(t)), \quad -l\cos(\theta(t))\big)\\ v(t) &= |\boldsymbol{x}'(t)| = l|\theta'(t)|.\end{aligned}$$

The gravitational potential energy of the mass is intuitively

$$\begin{aligned}V(t) &= mg\boldsymbol{x}_2\\ &= -mgl\cos(\theta(t))\end{aligned}$$

and the kinetic energy

$$\begin{aligned}T(t) &= \frac{1}{2}mv^2(t)\\ &= \frac{1}{2}lm\dot{\theta}^2(t),\end{aligned}$$

which together form the Lagrangian $L(t) = T(t) - V(t)$.

Our oscillatory driving force however is non-conservative and not associated with a potential, and is incorporated into the Lagrangian formalism as a generalised force.

$$\begin{aligned}Q(t) &= \boldsymbol{F}(t)\cdot\frac{\partial\boldsymbol{x}(t)}{\partial\theta(t)}\\ &= \boldsymbol{F}(t)\cdot\big(l\cos(\theta(t)), \quad l\sin(\theta(t))\big)\,.\end{aligned}$$

where $\boldsymbol{F}(t)$ is our vectorised driving force. Notice however that our right vector is orthogonal to the pendulum arm...

$$\big(l\cos(\theta(t)), \quad l\sin(\theta(t))\big)\cdot\boldsymbol{x}(t) = 0 \quad \forall t$$

and so is parallel (or anti-parallel) to our driving force, allowing us to write

$$Q(t) = F(t)\left|\big(l\cos(\theta(t)),\quad l\sin(\theta(t))\big)\right| = lF(t),$$

noting that we've not taken the absolute value of $F(t)$ to encapsulate direction.

The Euler-Lagrange equation for this system with parameter $\theta(t)$ is

$$\begin{aligned} Q(t) &= \frac{\partial}{\partial t}\left(\frac{\partial L(t)}{\partial \dot{\theta}(t)}\right) - \frac{\partial L(t)}{\partial \theta(t)} \\ lF(t) &= lm\ddot{\theta}(t) + mg\sin(\theta(t)). \end{aligned}$$

If we now substitute the small angle sine ($\sin(\theta(t)) \approx \theta(t)$) and therefore that $x_b(t) \approx l\sin(\theta)$, we're presented with the equation of motion for a driven (orthogonally to the arm), undamped pendulum.

$$F(t) = \frac{gm}{l}x_b(t) + m\ddot{x}_b(t).$$

B Linear Pendulum Gravitational Coupling Transfer Function

Consider an ideal frictionless linear pendulum of mass m and arm length l which swings in the x direction.

We model a gravitational-wave strain as an oscillatory, extraneous force acting at the pendulum's center of mass. Assuming the strain is small, a small angle approximation enables us to assume this force always acts orthogonally to the arm of the pendulum, in the x-vertical plane.

Letting x_b be the horizontal position of the mass relative to the suspension point, the equation of motion of our pendulum subject to a gravitational-wave strain (dervied in Appendix A) is

$$F(t) = Lm\ddot{h}(t) = \frac{gm}{l}x_b(t) + m\ddot{x}_b(t), \tag{52}$$

where we've also substituted the form of this force (Equation 1).

We move to frequency space by applying the Fourier transform to both sides of Equation 52, letting

$$X_b(f) = \mathcal{F}\{x_b(t)\} \qquad \text{and} \qquad H(f) = \mathcal{F}\{h(t)\} \tag{53}$$

where

$$\ddot{x}_b(t) \to -f^2 X_b(f) \qquad \text{and} \qquad \ddot{h}(t) \to -f^2 H(f). \tag{54}$$

This presents

$$-Lf^2 H(f) = \left(\frac{g}{l} - f^2\right) X_b(t). \tag{55}$$

The transfer function of the linear pendulum in response to a gravitational-wave strain is found by rearranging Equation 55 and substituting the linear pendulum critical frequency ${f_0}^2 = g/l$.

$$T(f) = \frac{X_b(f)}{LH(f)} = \frac{f^2}{f^2 - {f_0}^2}. \tag{56}$$

C Linear Pendulum Seismic Noise Equation of Motion

Consider a frictionless, unforced, linear pendulum of mass m and arm length l which swings in the x direction, which features a time-varying suspension position $x_t(t)$ and a consequentially varying mass position $x_b(t)$.

INSERT DIAGRAM

Assuming the angle ϕ between the pendulum arm and the vertical is kept small, we apply the small angle approximation and write

$$\phi(t) \approx \sin(\phi(t)) = \frac{x_b(t) - x_t(t)}{l}. \tag{57}$$

The position of the mass, given vectorially and noting the absolute vertical position to be arbitrary, is

$$\begin{aligned} \boldsymbol{r}(t) &= \big(xb(t), \quad -l\cos(\phi(t))\big) \\ &\approx \big(x_b(t), \quad -l\left(1 - \tfrac{1}{2}\phi^2(t)\right)\big) \end{aligned} \tag{58}$$

with velocity

$$\boldsymbol{v}(t) = \dot{\boldsymbol{r}}(t) = \big(\dot{x}_b(t), \quad l\dot{\phi}(t)\phi(t)\big)\,. \tag{59}$$

This allows for an expression of the kinetic energy of the mass as

$$\begin{aligned} T(t) &= \frac{1}{2}m|\boldsymbol{v}|^2 \\ &= \frac{1}{2}m\left(\dot{x}_b^2(t) + \frac{(x_b(t) - x_t(t))^2(\dot{x}_b(t) - \dot{x}_t(t))^2}{l^2}\right) \end{aligned} \tag{60}$$

and a potential (gravitational) energy of

$$\begin{aligned} V(t) &= mg\boldsymbol{r}_2(t) \\ &= glm\left(1 - \frac{(x_b(t) - x_t(t))^2}{2l^2}\right), \end{aligned} \tag{61}$$

which together constitute the Lagrangian

$$L = T + V.$$

The equation of motion is established by construction of the Euler-Lagrange equation and cancelling m. CITE

$$\begin{aligned} 0 &= \frac{\mathrm{d}}{\mathrm{d}t}\left(\frac{\partial L}{\partial \dot{x}_b}\right) - \frac{\partial L}{\partial x_b} \\ \implies 0 &= l^2\ddot{x}_b - (x_b - x_t)\left(gl + (\dot{x}_b + \dot{x}_t)^2 + (x_b + x_t)(\ddot{x}_b - \ddot{x}_t)\right) \end{aligned} \tag{62}$$

D Linear Pendulum Seismic Noise Transfer Function

Consider an ideal, frictionless linear pendulum of mass m and arm length l which swings in the x direction. Its response to seismic noise, modeled as small-angle oscillatory perturbation of the suspension point of the pendulum, is described by the equation of motion (derived in Appendix C)

$$l^2\ddot{x}_b - (x_b - x_t)\left(gl + (\dot{x}_b + \dot{x}_t)^2 + (x_b + x_t)(\ddot{x}_b - \ddot{x}_t)\right) = 0 \tag{63}$$

where x_b and x_t are the time-dependent x-positions of the bottom and top (the mass and suspension point) of the pendulum respectively, and g is the acceleration due to gravity near the Earth's surface.

We move to frequency space by Fourier transforming Equation 63, letting

$$X_i(f) = \mathcal{F}\{x_i(t)\}$$

(for each of $i = b, t$, imagined as the amplitude of the oscillations of the bottom and top of the pendulum respectively) where, by assuming these terms oscillatory, the n-th derivatives transform as

$$\mathcal{F}\{{x_i}^{(n)}(t)\} = (if)^n X_i(f).$$

This presents

$$gl(X_t - X_b) + (l^2 X_b + 2(X_b - X_t)^3)f^2 = 0. \tag{64}$$

Under the small angle approximation, we neglect any angle terms higher than second order, setting $(X_b - X_t)^3 \approx 0$. Also substituting the resonant frequency of a linear pendulum ${f_0}^2 = g/l$ CITE, we rearrange to find the transfer function as the ratio of the amplitude of the responding mass oscillations to that of the seismic vibrations.

$$T_s(f) = \frac{X_b(f)}{X_t(f)} = \frac{{f_0}^2}{{f_0}^2 - f^2}. \tag{65}$$

E Torsion Pendulum Seismic Response

F Torsion Pendulum Gravitational Coupling

G Rotational Stiffness of a Cylindrical, Linearly Elastic Cable

The rotational stiffness k is also known as the *couple per unit twist*; the torque causing longitudinal rotation induced by a unit of twist of the cable.

Under the assumption of a linearly elastic material, shear stress τ is linearly related to a shear strain γ by the shear modulus G_s [15];

$$\tau = G_s \gamma. \tag{66}$$

A cylinder of radius r_s subject to angle of longitudinal twist per unit length θ, experiences at every point parameterized by radius $\rho < r_s$ a shear strain of

$$\gamma = \rho\theta \tag{67}$$

and thus a shear stress of

$$\tau = G_s \rho \theta. \tag{68}$$

An infinitesimal cross-sectional area $\mathrm{d}A$ experiences an infinitesimal shear force

$$\mathrm{d}F = \tau \, \mathrm{d}A \tag{69}$$

and therefore a torque

$$\mathrm{d}T = \mathrm{d}F \rho = \tau \rho \mathrm{d}A. \tag{70}$$

The rotational torque on a cross-section of the cable is found by integration over the full cross-sectional area A of the cable.

$$T(\theta) = \int_A \tau \rho \, \mathrm{d}A \tag{71}$$

$$= G\theta \int_A \rho^2 \mathrm{d}A. \tag{72}$$

We recognise the integral expression of the polar moment of inertia of a uniform cylinder, and substitute its value for a circular cross-section [32].

$$T(\theta) = G_s \theta \frac{\pi {r_s}^4}{2}. \tag{73}$$

By assuming the rate of twist along the cable of length L_s is uniform, a total twist angle of $\phi = L_s \theta$ produces a total torque

$$T(\phi) = G_s \frac{\phi}{L_s} \frac{\pi {r_s}^4}{2}. \tag{74}$$

The rotational stiffness of our cylindrical, linearly elastic cable [16] is therefore

$$k = \frac{T(\phi)}{\phi} \tag{75}$$

$$= \frac{G_s \pi {r_s}^4}{2L}. \tag{76}$$